Revealing Mesoscale Ionomer Membrane Structure by Tender Resonant X-ray Scattering

Sintu Rongpipi,[1,2,§] Jonathan M. Chan,[1,2,§] Ashley Bird,[3,4] Guillaume Freychet,[5,6] Ahmet Kusoglu,[3] Gregory M. Su*[1,2]

*corresponding author: gsu@lbl.gov, Lawrence Berkeley National Laboratory, 1 Cyclotron Road, Berkeley, CA, 94720, United States
[1]Advanced Light Source, Lawrence Berkeley National Laboratory, Berkeley, CA 94720 United States
[2]Materials Sciences Division, Lawrence Berkeley National Laboratory, Berkeley, CA, 92720, United States
[3]Energy Conversion Group, Lawrence Berkeley National Laboratory, Berkeley, CA, 94720, United States
[4]Department of Chemical and Biomolecular Engineering, University of California, Berkeley, Berkeley, CA, 94720, United States
[5]National Synchrotron Light Source II, Brookhaven National Laboratory, Upton, NY, 11973, United States
[6]Université Grenoble Alpes, CEA, Leti, Grenoble, France
[§]These authors contributed equally to this work.

Keywords: resonant x-ray scattering, ionomer, membrane, nanostructure, polymer assembly

Abstract

Nafion, a perfluorosulfonic acid ionomer, has been well-studied for decades due to its key role as ion-conductive membranes in electrochemical energy conversion and storage applications. When hydrated, this membrane phase separates into a complex, hierarchical nanostructure with hydrophilic domains that facilitate ion transport. Hard x-ray scattering has been a resourceful technique in understanding Nafion due to its capabilities in capturing the ionomer's nanophase separated structure, which gives rise to contrast between polymer and water domains. More recently, resonant x-ray scattering, which tunes to elemental absorption edges to provide specificity on constituent elements, has been explored to highlight key interactions related to the sulfonic acid groups within its structure. Here, we study Nafion nanostructure by combining hard x-ray scattering and tender resonant x-ray scattering (TReXS) at the sulfur K-edge to reveal a mesoscopic feature corresponding to a correlation length of approximately 40 nm that has been challenging to resolve with hard x-ray studies. Additionally, we study the effect of the dispersion solvent composition that plays a key role in the formation of this mesoscale feature. Notably, TReXS can attain high contrast to decipher this mesoscale morphology even for dry polymer membranes under vacuum, which typically have reduced contrast for hard x-rays. We find that the correlation length of this mesoscale feature decreases with increasing water fraction in the dispersion, which is the opposite trend exhibited by the smaller intercrystalline feature in the same membranes. This study showcases the utility of TReXS to uncover multi-scale morphological details in functional polymers that are not always revealed by other methods like hard x-ray scattering. We illustrate this with Nafion, which is a relevant ion-conducting polymer for electrochemical technologies.

Introduction

Perfluorosulfonic acid (PFSA) ionomers have been a popular choice of membranes for a variety of electrochemical energy conversion and storage applications due to their high proton conductivity and chemical, thermal, and mechanical stability.[1–7] These polymers are composed of a hydrophobic perfluorinated backbone with hydrophilic sulfonic acid-terminated side chains, which, when hydrated, phase separate into interconnected nano-domains that facilitate ion conduction throughout the system. The transport of species through these materials depends strongly on this phase-separated morphology, particularly the size, connectivity, and chain ordering, which determine the transport pathways of charged (ion) and uncharged (water) species. The formation of this final morphology is not entirely understood, with numerous models and theories to explain this underlying phenomenon, [8–13] and the morphology is even

more complicated and affected by various processing parameters that can affect it.[14–16] Several recent studies have focused their attention specifically on the effect of dispersion solvent composition on the final morphology of PFSAs,[14,17–22] due to its impact on dispersion-phase aggregation and bulk-phase assembly and to its relevance in the manufacturing of solution-cast membranes.[23,24]

Thus far, the hierarchical morphology of PFSA ionomers have been difficult to quantify, in part due to the large range in length scales the structure spans, from molecular-scale signatures to larger, mesoscopic phase-separated features. Additionally, because their nanostructure is driven by so many different factors, such as hydration, environment, casting methods and parameters,[1] our understanding of this structure is best understood by focusing on one of these factors at a time. X-ray scattering has been a robust and widely employed technique in studying PFSAs and has probed angstrom-level features relevant to polymer chain packing within crystallites up to tens of nanometers to investigate domain spacings between hydrophilic domains and semicrystalline regions.[5,24–29] While much attention has focused on the impact of hydration on the nanostructure of PFSAs, more recently, questions about the effect of solvent composition on PFSA morphology has come into prominence. This is relevant because solvent-casting methods are used to produce PFSA membranes in commercial devices, such as in fuel cells, electrolyzers, and flow batteries.[14,30] X-ray scattering has been particularly helpful in answering questions about the effect of dispersion solvent composition on PFSA morphology, demonstrating how larger hydrophilic domains and a greater degree of connectivity among these domains are found for membranes cast from solvents with a higher water fraction. Larger and more connected hydrophilic domains are advantageous in PFSAs as they result in a more ion conductive material.[18,22,31] Dynamic light scattering (DLS), transmission electron microscopy (TEM) and coarse-grained molecular dynamics simulation have provided key insight on the role of water/alcohol content in dispersion solvents on the aggregation behavior of PFSAs, showing larger rod-like aggregates form in less polar solvent environments, which plays a major role in the final bulk polymer membrane morphology.[17,19,22] Previous studies on ionomers have largely focused on the formation and behavior of nanoscale features,[14,18] but so far, the influence of dispersion content on larger, mesoscale features is not as well understood.

X-ray scattering has contributed significantly to understanding PFSA ionomer morphology, largely due to its ability to probe the broad range of relevant length scales (from molecular to mesoscale features) and its ease in application to ionomer systems. The use of hard x-ray scattering for PFSAs is well-studied, and the key morphological signatures seen using this technique are relatively well-determined.[1] Typically, these features are, from smallest to largest in real space, (1) the chain packing within crystallites in the semi-crystalline backbone domains, (2) the domain spacing between ion-containing hydrophilic regions, especially in a hydrated state, and (3) the domain spacing between semicrystalline regions within the polymer matrix. Hard X-ray scattering contrast is based on differences in electron density. This can result in limited contrast in soft materials that are composed of light elements, as is the case with PFSAs. Energy-resolved resonant x-ray scattering (ReXS) can achieve much greater scattering contrast between polymers and other organic materials by tuning the energy near elemental absorption edges, where contrast can vary greatly due to differences in absorption. This enables ReXS to achieve high scattering contrast between polymer domains with different elemental compositions, and even between domains or functional groups containing the same elements but with different bonding environments. For polymers and soft materials, most of the elemental core-level absorption edges fall within the soft (150-2000 eV) or tender (2000-7000 eV) x-ray regimes.[32,33] There has only been limited work so far using tender resonant x-ray scattering (TReXS) near the sulfur K-edge to probe nanostructure in PFSA membranes, [14,18,25,34,35] and this work focused on the effect of PFSA side chain chemistry and side chain modification on nanoscale morphology, evidenced by changes to the ionomer peak in the 0.1-0.3 $Å^{-1}$ range. This established TReXS as a unique tool to reveal new morphological details by probing variations in sulfur content in industrially-relevant PFSA membranes (10-200 micron thick). Here, we build upon previous studies to show how TReXS can also uncover new details of ionomer membrane morphology at larger, mesoscopic length scales.[25,34]

While most technologies employing ionomer membranes use them in hydrated environments, there is a practical interest in developing and examining membranes that operate in drier or hotter conditions as well as a fundamental interest in understanding the structure of an ionomer's functional groups (e.g. micelle formation) in a low-hydration environment because it better highlights the polymer-ion interactions, which are otherwise shielded by solvation and water uptake.[1,36] Hard x-ray scattering has proven to be a suitable tool to investigate the nanostructure of phase-separated ionomer membranes, especially under hydration, which gives rise to enhanced scattering contrast due to the electron density differences between the polymer and hydrophilic (ion-rich, water-filled) domains. Nevertheless, in the absence of sufficient water molecules, as is the case for dry membranes, the lack of x-ray scattering contrast renders hard x-ray scattering less effective for resolving the polymer-ion structure, in particular, the distribution of ionic moieties in the hydrophobic semicrystalline matrix. Capturing such information and resolving the chemical interactions, however, require the ability to access chemical structure information at relevant absorption edges. This is where the unique capabilities of ReXS, including TReXS, can help answer these questions.

In this study, we employ resonant x-ray spectroscopic and scattering techniques near the sulfur K-edge to investigate the nano- to mesoscale morphology of Nafion membranes. We examine the effect of water content within the dispersion solvent on self-assembly of domains within resulting membranes. Due to extensive research history and comprehensive understanding of Nafion's mechanical, conductive, and transport properties, this functional material serves as an excellent model system for carrying out these x-ray experiments. Using TReXS, we observe a previously overlooked peak at the sulfur K-edge corresponding to a feature of approximately 40 nm in size, which has been difficult to resolve thus far using hard x-ray scattering. Notably, we observe that increasing the amount of water in the dispersion leads to a decrease in the characteristic length scale of this mesoscopic feature, the opposite effect that is seen and previously reported for the intercrystalline feature. By drawing similarities to studies using neutron and ultra-small angle x-ray scattering, we provide a possible origin and mechanism for the formation of this mesoscale structural feature. Beyond accessing elemental sensitivity using TReXS, this technique positions us to study dry Nafion membranes under vacuum, which has not been often investigated due to the limited scattering contrast under highly dehydrated conditions. Focusing on this infrequently studied sample and experimental environment and successfully capturing new information on Nafion nanostructure, this work demonstrates the strength of ReXS as a complementary tool to the more conventional hard x-ray scattering. This work expands on our knowledge of PFSA membrane morphology by employing both techniques to explore the origin and behavior of the often-missed mesoscale feature, establishing the necessity of utilizing multiple energies in tandem.

Methods

Ionomer dispersions

4 wt % of Nafion (PFSA) was dispersed in solvents of varying ratios of water to n-propanol (nPA) ranging from 30 wt % water to 90 wt % water (balance nPA). The dispersions were prepared by diluting a stock 20 wt % dispersion (Nafion™, D2021, equivalent weight of 1100 g polymer/mol sulfonic acid groups, Ion Power, Inc.) to the target concentration using water and nPA, considering the native solvent in the stock dispersion. Upon dilution, dispersions were mechanically mixed and then sonicated for 30 min in a bath sonicator (Branson) equipped with a custom temperature control system to maintain room temperature.

Membranes cast from ionomer dispersions

Membranes were cast from the dispersions described above. The dispersions were poured into custom-made glass wells using the same mass of the ionomer. They were heated at 35 °C under vacuum for 1 h and annealed at 150 °C for an additional hour, before slowly cooling back to room temperature overnight. They were then carefully removed from the glass wells, and the thickness of all membranes was measured to be *ca*. 15 μm in dry state using a thickness gauge (Heidenhain).

Near edge X-ray absorption fine structure (NEXAFS) spectroscopy

NEXAFS spectra were collected in fluorescence yield (FY) mode at the Soft Matter Interfaces (SMI) beamline 12-ID-C of the National Synchrotron Light Source II (NSLS-II), at the Brookhaven National Laboratory (BNL).[1] Spectra from 2452 eV to 2507 eV covering the sulfur K-edge were collected within a single scan. The X-ray fluorescence intensity was recorded using a Pilatus 300K-W detector, consisting of 172x172 μm^2 pixels in a 1475 × 195 array, mounted at a fixed distance of 0.275 m from the sample position. To limit contamination of the fluorescence yield intensity by any scattered X-rays, the Pilatus detector was moved horizontally on a fixed arc to an angle of 52 degrees. The measurements were performed in a vacuum chamber and the NEXAFS spectra were normalized with respect to the direct beam flux, measured on diamond beam position monitors.

X-ray scattering measurements

Hard X-ray scattering measurements were collected at SMI beamline 12-ID-C of NSLS-II. Small angle X-ray scattering (SAXS) data were collected using 16.1 keV X-rays and a Pilatus 1M detector consisting of 172x172 μm^2 pixels with a sample-detector distance of 8.3 m to cover a q range of 0.003 $Å^{-1}$ to 0.124 $Å^{-1}$. Wide angle X-ray scattering (WAXS) data were collected using a Pilatus 300K-W detector, consisting of 172x172 μm^2 pixels with a sample-detector distance of 280 mm. To cover a q range of 0.038 $Å^{-1}$ to 7.050 $Å^{-1}$ the vertically oriented elongated detector was moved horizontally on a fixed arc at 0, 20, and 40 degrees. Images were later visualized in Xi-CAM software[37] and stitched using custom code.

Sulfur K-edge TReXS measurements of membranes were collected at the Soft Matter Interfaces (SMI) beamline 12-ID-C at the NSLS-II. X-ray scattering patterns were recorded on a Pilatus 300K-W detector, consisting of 172x172 μm^2 pixels in a 1475 × 195 array, mounted at a fixed distance of 0.275 m from the sample position. To cover the range of scattering angles desired, the vertically oriented elongated detector was moved horizontally on a fixed arc, from 0 to 45.5 degrees with 6.5 deg steps. Scattering patterns, recorded in-vacuum, were measured at energies across the sulfur K-edge (2542 to 2507 eV). The spot size at the sample was 20 μm by 200 μm (vertical by horizontal). Images were visualized and stitched as mentioned above.

Results and Discussion

To study the complex, hierarchical morphology of PFSAs, we performed x-ray spectroscopy and scattering on Nafion membranes using energies near the sulfur K-edge. Near edge x-ray absorption fine structure (NEXAFS) spectroscopy measurements in fluorescence yield (FY) mode taken around the sulfur K-edge show a main absorption feature between 2.480-2.487 keV. This spectrum (Figure 1a) is similar to previously reported results for Nafion, where the larger peak near 2.480 keV is associated with a transition to a $\sigma^*_{S\text{-}C}$ antibonding orbital and the lower intensity peak that follows is associated with a $\pi^*_{S\text{-}O}$ transition.[25,38–41] We believe the small peak that appears in the pre-edge (~2.475 keV) is an artifact, likely due to impurities within the membrane and/or bright pixels on the detector. Tender resonant x-ray scattering (TReXS) measurements were also taken for Nafion. Absorption near the sulfur K-edge will modulate the scattering contrast around these energies (scattering contrast calculation shown in Supporting Information, Figure S1). Figure 1b shows the radially integrated 1D scattering profiles at 16.10 keV (hard x-ray), 2.449 keV (pre-edge), 2.482 keV (on-edge), and 2.504 keV (post-edge) for a Nafion membrane cast from a dispersion with 30% water balanced with n-propanol (nPA). The 2D scattering data is shown in Figure S3. The 1D profiles at 16.10 keV, 2.449 keV, and 2.504 keV display two distinct peaks: one around q = 0.06 $Å^{-1}$ indicating the intercrystalline domain spacing (Peak 2), and another at q = 0.2 $Å^{-1}$, indicating the hydrophilic domain spacing (Peak 3).[1,14,25] We also observe another peak at approximately q = 0.015 $Å^{-1}$ at the sulfur absorption edge (2.482 keV), which corresponds to a feature on the length scale of approximately 40 nm. This mesoscale feature (Peak 1) is most apparent in scattering measurements performed at energies near where the main absorption peak in the NEXAFS spectra is observed, highlighting the enhanced contrast near these on-resonance energies and the potential of TReXS to reveal sulfur-specific behavior within the assembled structure in Nafion.

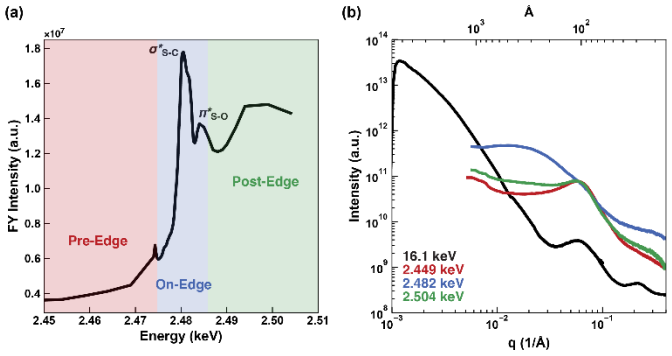

Figure 1: (a) Fluorescence yield (FY) sulfur K-edge NEXAFS spectra of a Nafion membrane cast from a dispersion solvent containing 30% water (remaining is nPA). (b) Radially integrated 1D scattering profiles of a Nafion membrane cast from a dispersion solvent containing 30% water (remaining is nPA) at X-ray energies 16.1 keV (hard X-ray), 2.449 keV, 2.482 keV, and 2.504 keV (tender X-ray near sulfur K-edge). Scattering of the Nafion membrane at energies near the sulfur K-edge absorption peak reveals a new mesoscale morphological feature (~40 nm). Energies were calibrated based on methods detailed in the SI.

The emergence of the peak at q = 0.015 Å^{-1}, which we will refer to as the mesoscale peak, at the sulfur K-edge implies some interactions and distribution of the sulfonic acid groups on a larger length scale than the typical intercrystalline domain spacings. A similar feature, noted in other studies as the ultra-small angle scattering (USAS) upturn, has been observed in ultra-small angle x-ray scattering (USAXS) and neutron scattering.[29,42–45] In these studies, this feature has been associated with chemical compositional inhomogeneities within the polymer matrix.[43,46] These inhomogeneities likely arise early in membrane formation during the ionomer aggregation processes in dispersion. They remain in an elongated semi-crystalline form when the bulk polymeric structure forms during casting, and the regions of crystallinity are present throughout the polymer matrix. Factors such as uneven drying and swelling drive the spacings between these aggregates and have been shown to affect the spacing of this feature. Because the mesoscale peak is only apparent at the sulfur K-edge, it can be inferred that the increased sensitivity to the inhomogeneities of the crystalline domains are related to some apparent order of sulfur-rich domains.

To gain a better understanding of the origin of the mesoscale peak, we investigated the energy dependence of the scattering features and probed the element-specific contributions and sulfur density variations through the system. We collected data through the range of 2.449 to 2.504 keV, specifically tracking characteristics of the mesoscale peak (Peak 1), the intercrystalline peak (Peak 2), and the ionomer peak (Peak 3). In Figure 2a, we plot the 1D scattering profiles at energies throughout this range for the membrane cast from a 30% water dispersion. We also determined the intensity of each peak by integrating over the peak regions for each feature and plotted the intensities as a function of energy for each peak, which predictably display strong energy modulations near the absorption edge (Figure 2b).[47,48] Here, the ionomer peak (peak 3) displays an intensity vs. energy behavior similar to the NEXAFS spectra near the sulfur K-edge, while the mesoscale and intercrystalline peaks display a distinct and different behavior. This suggests some sulfur-based contrast mechanism for these two peaks (mesoscale and intercrystalline) beyond the fluorescence effects from absorption. For the ionomer peak, it is difficult to draw significant conclusions based on its similar behavior to the NEXAFS spectra and its intensity is similar to the fluorescence background. These results suggest that the increased scattering contrast in both the mesoscale peak and intercrystalline peak arises from variations in density and distribution of sulfur at these relevant features. Specifically, the difference in how sulfur is distributed in the amorphous fraction of the semicrystalline regions leads to heightened contrast of the intercrystalline peak near the sulfur K-edge. Similarly, although we do not have a full understanding of the mesoscale peak, its appearance near the

sulfur K-edge provides a hint that it captures information on the sulfur content distribution through the system at this length scale (~40 nm), which we will discuss in more detail later.

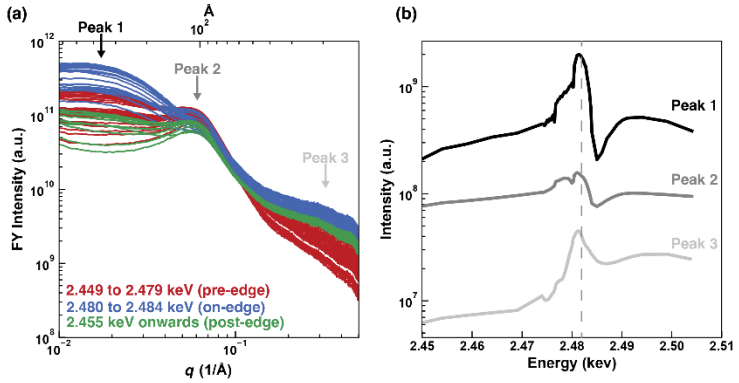

Figure 2: (a) Radially integrated 1D scattering profiles from a Nafion membrane cast from a dispersion solvent containing 30% water (remaining is nPA) at X-ray energies across the sulfur K-edge. (b) Variation of scattering intensity with energy for scattering peaks observed at q ~0.015 $Å^{-1}$ (Peak 1), ~0.06 $Å^{-1}$ (Peak 2), and ~0.2 $Å^{-1}$ (Peak 3). Scattering peaks from the Nafion membrane have distinct energy dependence across the sulfur K-edge.

Previous studies explored the effects of water/alcohol content in ionomer dispersion solvents, where the polarity drives the conformation of the polymer chains, affecting morphology and macroscopic properties. For example, work by Berlinger et al. demonstrated that a higher polarity solvent results in more elongated chain conformation with sulfonic acid groups oriented outwards, whereas ionomer chains in a more nonpolar solvent form coiled structures with sulfonic acid groups oriented inward to form "inverted micellar" structures.[17] Chain conformation affects aggregation by forming either more ordered, rod-shaped aggregates or loose, thicker aggregates. The effect of chain conformation and aggregation behavior is preserved even in bulk ionomer membranes after casting, where domain sizes, degree of crystallinity, and morphology within hydrophilic and hydrophobic domains are affected.[6,17] Because solvent composition drives the orientation of sulfonic acid groups on the single-chain level, which further extends to the aggregate and bulk polymer level, we opted to study membrane morphology as a function of varying dispersion composition using TReXS around the sulfur K-edge. We probed the mesoscale feature seen at the sulfur K-edge for various membranes cast from dispersions with 30%, 50%, 70%, and 90% water, balanced with nPA. The effect of the dispersion solvent composition was studied by fitting the mesoscale peak from each of the 1D scattering profiles to a Gaussian distribution to extract the amplitude of the feature (Figure 3a). The 1D profiles for each dispersion composition are shown in Figure S4. We observe that the highest amplitude is reached near the on-edge energy at approximately 2.481 keV, suggesting a strong dependence of this feature on the sulfur content. The amplitude also increases with lower water content in the dispersion (Figure 3b). From the single-chain perspective, in a solvent with lower water content, the hydrophilic sulfonic acid groups along the chain would be oriented inward. If this configuration is even moderately conserved in the bulk, this would lead to more discrete regions with greater sulfur density, which may explain the increase in amplitude of the mesoscale scattering peak for membranes cast from dispersions with a lower water fraction. Alternatively, in a more polar solvent, which more favorably interacts with sulfonate groups, elongated chains would not have a preferential distribution of sulfonic acid groups towards the interior of the coil and aggregates in solution, and therefore this could lead to a more homogeneous sulfur distribution in the cast membrane, resulting in a disrupted periodicity and therefore a weaker scattering peak.

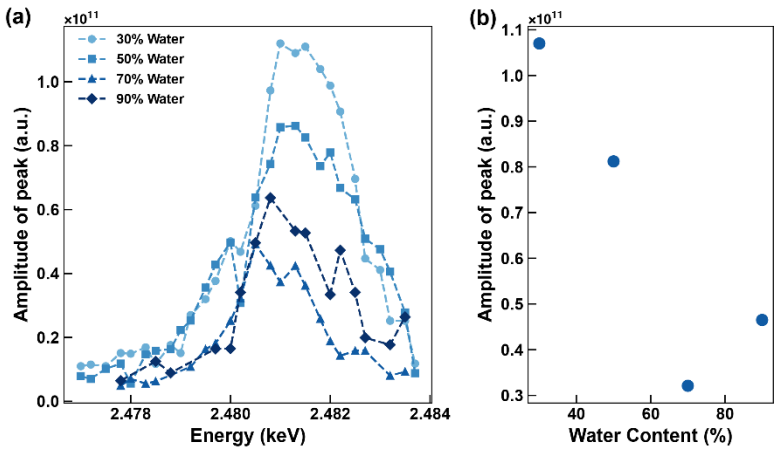

Figure 3: (a) Variation of amplitude of the mesoscale peak with X-ray energy. The amplitude of the mesoscale peak ($q \sim 0.015$ Å^{-1}) was calculated by fitting the peak with a Gaussian function after background subtraction with a linear background in the region from $q \sim 0.008$ Å^{-1} to $q \sim 0.04$ Å^{-1}. (b) Average amplitude of the mesoscale peak for energies from 2.481 to 2.484 keV is plotted as a function of dispersion water content. The evolution of the mesoscale peak depends on water content of the dispersion solvent from which a membrane is cast.

We further examined the effect of solvent composition on morphology by analyzing the change in characteristic length scale of the mesoscale and intercrystalline peaks by extracting their peak positions from the Gaussian fits. Notably, we observe that increasing the amount of water in the dispersion results in the characteristic length scale associated with the mesoscale feature decreases, while the characteristic length scale of the intercrystalline peak increases (Figure 4). The behavior of the intercrystalline peak is consistent with previous studies on morphology with varying dispersion composition, which is driven by aggregation behavior in the dispersion state.[18] The opposite relationship between the amount of water in the dispersion and the domain spacing for the mesoscale peak compared to the intercrystalline peak is somewhat surprising, but nevertheless provides insight to better understand the mechanism underlying the formation of the complex hierarchical morphology of PFSA membranes. We postulate reasons for this result by discussing the mechanism of membrane morphology development from dispersion.

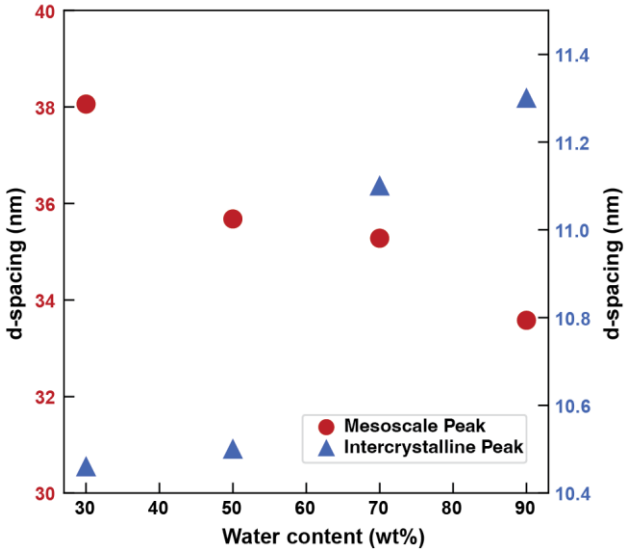

Figure 4: Variation of the characteristic length scale of the mesoscale peak ($q \sim 0.015$ Å^{-1}) and the intercrystalline peak ($q \sim 0.06$ Å^{-1}) with water content (wt%) in the dispersion solvent (balance is nPA). The characteristic length scales were calculated by fitting the peaks with a Gaussian function after background subtraction. For the mesoscale peak, the reported characteristic length scale is taken from the scattering profile at 2.481 keV where the X-ray energy

is maximized. The reported characteristic length scale for the intercrystalline peak is taken as an average calculated from the scattering profiles across 2.449 to 2.470 keV. The characteristic length scale of the mesoscale peak and the intercrystalline peak depend on the amount of water in the dispersion solvent from which the membrane is cast.

Guided by our results, we propose a mechanism for morphology formation in the Nafion membranes that begins with our understanding from a single-chain level. A schematic explaining this mechanism is shown in Figure 5. It is understood that the polarity of the dispersion solvent drives the conformation and distribution of sulfonic acid groups for single chains. At this dispersion state, these chains will aggregate, and the aggregates preserve some of the chain properties in its size, shape, and packing. For example, in a polar solvent containing more water, where the chains take on an elongated conformation, the aggregates are expected to be more rodlike and more efficiently packed, forming longer, thinner structures with the ionic groups oriented outward. This corresponds to larger intercrystalline spacing but with lower mesoscale spacing due to efficient packing at longer length scales. In a dispersion with lower water concentration, however, the chains likely take on a more coiled structure, where the sulfonic acid groups are oriented inward and distributed more densely at its core. The resulting aggregate would be larger and more loosely packed, resulting in higher mesoscale domain spacing. This likely explains why the characteristic length scale or domain separation associated with the mesoscale feature increases with decreasing amount of water in the dispersion (from water-rich to alcohol-rich). The sulfonic acid groups would also be oriented towards the center of the aggregate instead of the outside, leading to more well-defined regions of greater sulfur density, and this may account for the greater amplitude of the mesoscale scattering feature at “on-resonance” energies for membranes cast from lower water content dispersions. These distinct aggregation characteristics drive the resulting bulk membrane morphology, as morphological aspects of the ionomer in dispersion are retained while solvent evaporates and solid-state membranes are formed.

The mesoscale peak that TReXS reveals has gone largely unnoticed using hard x-ray scattering, so it is likely that this is related to the density distribution of sulfur within the system on the tens of nanometers scale. Because the dispersion solvent composition may affect the distribution of sulfonic acid groups within ionic moieties, chains, and aggregates, some amount of this effect could carry through to the bulk membrane state. Although we do not necessarily expect the bulk Nafion to entirely retain the structure and sulfonic acid group distribution from its aggregate state, it is possible this is at least partially retained as bundles or grains with semi-distinct boundaries or edges in a mesoscale domain network. Under this assumption, the mesoscale peak we see through TReXS may be capturing these polymer bundles. The increase in domain spacing of the mesoscale peak as the amount of water in the dispersion decreases is therefore consistent with previous work, which has shown the formation of larger aggregates occurs in dispersions when water content is decreased.[18]

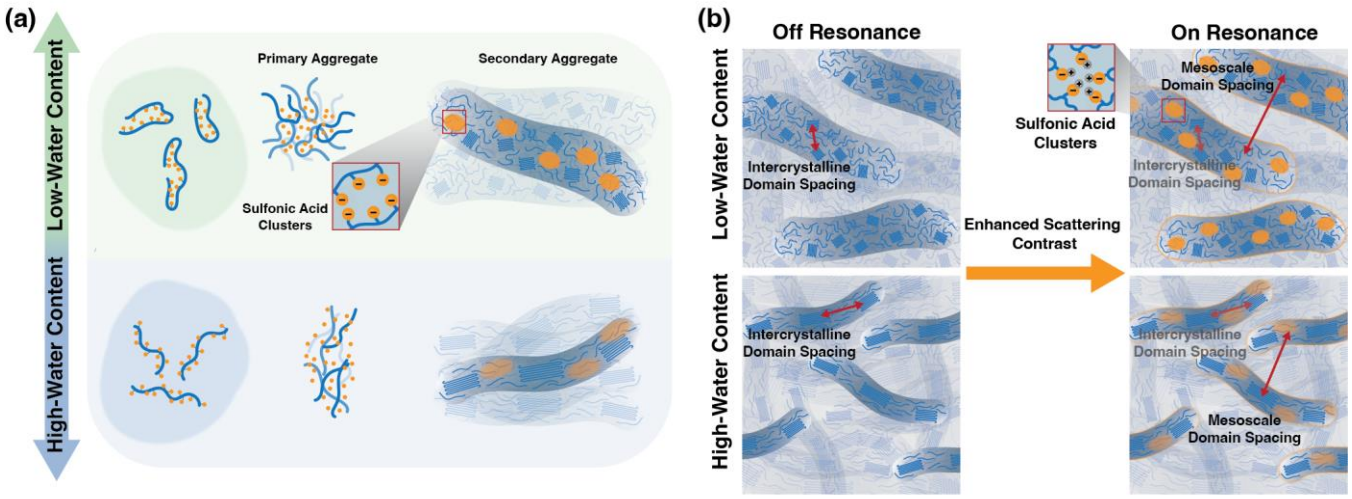

Figure 5: Schematic of Nafion aggregation in dispersion and its connection to bulk membrane hierarchical morphology. (a) Chain formation is driven by water content, either giving rise to micellar structures in low-water content dispersions or elongated chains in high-water content dispersion. These conformations drive the character of aggregates, either as oriented or random clusters within primary aggregates. As primary aggregates combine from electrostatic interactions, they form secondary aggregates that have a size and orientation dependent on the characteristics of their previous form as primary aggregates. (b) As these secondary aggregates form bulk polymer membranes, this aggregate structure is hypothesized to be preserved in some fashion as loose bundles, and their size and ordering are determined by the size and order of the secondary aggregates. These bundles are more clearly seen in TReXS at the sulfur K-edge. Increased contrast occurs in membranes formed from dispersions with less water due to the inhomogeneous distribution of sulfonic acid groups that arise from the micellar structure of Nafion chains in the dispersion state.

By studying this mesoscale feature and understanding the structure-property relationship, there is great potential in designing PFSA membranes for electrochemical applications, specifically because it can lead to improving the conductive and transport properties of these materials. A recent modeling study by Crothers et al. showed that the hydrophilic domain distribution at mesoscales affects the various microscale, domain-level transport modes dissimilarly, resulting in different distributions of transport coefficients for water and protons.[49] Furthermore, they revealed through transport simulations that the transport pathways for water and protons may not always be the same, which opens possibilities for controlling transport functionality or selective ion transport in ionomer systems through their mesoscale features. While such effects are inferred in structure-property investigations of different ionomers supported by hard x-ray scattering,[18,25,35,50–52] the lack of complete structural information at mesoscales, especially regarding information on the distribution of sulfur in ionic domains, created a gap in understanding and implementing of such design rules. The technique presented here begins to fill this gap by providing missing information at the mesoscale. The ability to obtain and resolve structural information at multiple length scales could provide not only insights into the processing, aging, and thickness effects in relation to dispersion or environmental changes, as discussed in literature,[14,30,35,53–56] but also a means to eventually tune structure-driven functionality in membranes.

In this study, we demonstrated the role TReXS can play as a complementary technique to conventional hard x-ray scattering by highlighting its ability to reveal features that are often not seen when using non-resonant energies. Although this work only highlights one case within specific parameters, there is much more potential of TReXS in the field of PFSA ionomer membranes. So far in this area, researchers have studied effects of chemical structure on nanoscale structures within PFSAs or microscopic features at the interfaces using surface-sensitive techniques. However, resolving chemical structure at these length

scales have been nascent, especially with x-ray techniques. In this work, we focused on the effect of dispersion solvent composition on morphology features of dispersion-cast Nafion membranes in the meso- and nanoscale range. Future work should expand to uncover relationships between equivalent weight and molecular weight on self-assembly and structure, which has been shown in simulation studies on PFSAs.[57,58] Additionally, there are limitations with using TReXS to study systems in liquid or solution states because vacuum is often used at these lower x-ray energies and the penetration depth is limited to a relatively thin solution cross section. However, new capabilities in resonant x-ray scattering are being developed, and future work to probe ionomer aggregation behavior in dispersions using TReXS would help to better understand the connections between ionomer conformations in dispersion and membrane morphology. Dry-state considerations are also valuable in studying high temperature membranes and alternative acidic proton conductors,[55] and TReXS is well-suited for these studies. By further establishing this platform of element-specific nanoscale characterization for vacuum state, dry or anhydrous membranes, we open new avenues to better understand the multi-scale structures of ionomers.

Conclusion

This study demonstrates the enhanced characterization capabilities with the dual use of hard and tender x-ray scattering and with the unique environment of dry Nafion membranes in vacuum. From TReXS at the sulfur K-edge, we observe the typical peaks (intercrystalline and ionomer peaks) as well as a mesoscale peak that corresponds to a feature of approximately 40 nm in domain size. Although this feature has often eluded researchers in past hard x-ray experiments, there has been some evidence for its presence in ionomers as shown in USAXS and SANS studies. By directly investigating the impact of dispersion solvent composition on the behavior of this mesoscale peak, we find that the peak position shifts with changes in dispersion water concentration, namely dispersions with more water results in a smaller domain spacing while dispersions with less water (more alcohol) result in a larger domain spacing. From this observation, we speculate that the mesoscale peak arises due to the preservation of secondary aggregates during the formation of the polymer membrane from dispersion casting. This feature is only weakly related to aggregation as loose bundles in the bulk state and manifests as regions of higher sulfur content throughout the system. Because this feature arises as an effect of aggregation, and because aggregation effects lead to an inhomogeneous distribution of sulfonic acid groups, we believe this accounts for the increased contrast acquired through scattering near the sulfur K-edge. Ultimately, this study shows the ability of TReXS, and ReXS in general, to reveal subtle morphology details within functional membranes and the advantage of complementary hard and tender x-ray scattering to build a deeper understanding of complex nanostructures within polymer materials.

Acknowledgements

This work was supported by the Laboratory Directed Research and Development Program of Lawrence Berkeley National Laboratory under U.S. Department of Energy Contract No. DE-AC02-05CH11231. This work was also supported in part by the Hydrogen and Fuel Cell Technologies Office (HFTO), Office of Energy Efficiency and Renewable Energy, U.S. Department of Energy (DOE) through the Million Mile Fuel Cell Truck (M2FCT) consortia, technology managers G. Kleen and D. Papageorgopoulos under contract no. DE-AC02–05CH11231. A.B. acknowledges support from the National Science Foundation Graduate Research Fellowship Program under Grant No. DGE 1752814. This research used the Soft Matter Interfaces (SMI) beamline at the National Synchrotron Light Source II, a U.S. DOE Office of Science User Facility operated by Brookhaven National Laboratory under Contract #DE-SC0012704.

Supporting Information

The Supporting Information is available free of charge at https://pubs.acs.org/

- Scattering contrast calculations, NEXAFS data of PFSA membranes cast from dispersions of different water content, representative sulfur K-edge 2D TReXS images, radially integrated scattering profiles for PFSA membranes at energies across the sulfur K-edge, representative

background subtraction, intercrystalline peak amplitude vs. energy for PFSA membranes cast from different water content dispersions

References

(1) Kusoglu, A.; Weber, A. Z. New Insights into Perfluorinated Sulfonic-Acid Ionomers. *Chem Rev* **2017**, *117* (3), 987–1104. https://doi.org/10.1021/acs.chemrev.6b00159.

(2) Hamrock, S. J.; Yandrasits, M. A. Proton Exchange Membranes for Fuel Cell Applications. *Polymer Reviews* **2006**, *46* (3), 219–244. https://doi.org/10.1080/15583720600796474.

(3) Perry, M. L.; Weber, A. Z. Advanced Redox-Flow Batteries: A Perspective. *J Electrochem Soc* **2016**, *163* (1), A5064–A5067. https://doi.org/10.1149/2.0101601jes.

(4) Kusoglu, A. Ionomer Thin Films for PEM Fuel Cells. *ECS Meeting Abstracts* **2018**, *MA2018-01* (27), 1584–1584. https://doi.org/10.1149/ma2018-01/27/1584.

(5) Kusoglu, A.; Cho, K. T.; Prato, R. A.; Weber, A. Z. Structural and Transport Properties of Nafion in Hydrobromic-Acid Solutions. *Solid State Ion* **2013**, *252*, 68–74. https://doi.org/10.1016/j.ssi.2013.05.008.

(6) Holdcroft, S. Fuel Cell Catalyst Layers: A Polymer Science Perspective. *Chemistry of Materials* **2014**, *26* (1), 381–393. https://doi.org/10.1021/cm401445h.

(7) Cassir, M.; Meléndez-Ceballos, A. *Fuel Cells: A General Overview, Applications and Future Trends*; 2016. https://doi.org/10.1002/9781118906842.ch15.

(8) Kusoglu, A.; Dursch, T. J.; Weber, A. Z. Nanostructure/Swelling Relationships of Bulk and Thin-Film PFSA Ionomers. *Adv Funct Mater* **2016**, *26* (27), 4961–4975. https://doi.org/10.1002/adfm.201600861.

(9) Gierke, T. D.; Munn, G. E.; Wilson, F. C. Morphology in Nafion Perfluorinated Membrane Products, as Determined by Wide- and Small-Angle X-Ray Studies. *Journal of polymer science. Part A-2, Polymer physics* **1981**, *19* (11), 1687–1704. https://doi.org/10.1002/pol.1981.180191103.

(10) Loppinet, B.; Gebel, G. Articles Rodlike Colloidal Structure of Short Pendant Chain Perfluorinated Ionomer Solutions. *Langmuir* **1998**, *14*, 1977–1983.

(11) Gebel, G. Structural Evolution of Water Swollen Perfluorosulfonated Ionomers from Dry Membrane to Solution. *Polymer (Guildf)* **2000**, *41*, 5829–5838.

(12) Kreuer, K. D.; Portale, G. A Critical Revision of the Nano-Morphology of Proton Conducting Ionomers and Polyelectrolytes for Fuel Cell Applications. *Adv Funct Mater* **2013**, *23* (43), 5390–5397. https://doi.org/10.1002/adfm.201300376.

(13) Hsu, W. Y.; Gierke, T. D. *Ion Transport and Clustering in Nafion Perfluorinated Membranes*; 1983; Vol. 13.

(14) Dudenas, P. J.; Kusoglu, A. Evolution of Ionomer Morphology from Dispersion to Film: An in Situ X-Ray Study. *Macromolecules* **2019**, *52*, 7779–7785. https://doi.org/10.1021/acs.macromol.9b01024.

(15) Kusoglu, A.; Kushner, D.; Paul, D. K.; Karan, K.; Hickner, M. A.; Weber, A. Z. Impact of Substrate and Processing on Confinement of Nafion Thin Films. *Adv Funct Mater* **2014**, *24* (30), 4763–4774. https://doi.org/10.1002/adfm.201304311.

(16) Silva, R. F.; De Francesco, M.; Pozio, A. Solution-Cast Nafion® Ionomer Membranes: Preparation and Characterization. *Electrochim Acta* **2004**, *49* (19), 3211–3219. https://doi.org/10.1016/j.electacta.2004.02.035.

(17) Berlinger, S. A.; McCloskey, B. D.; Weber, A. Z. Inherent Acidity of Perfluorosulfonic Acid Ionomer Dispersions and Implications for Ink Aggregation. *Journal of Physical Chemistry B* **2018**, *122* (31), 7790–7796. https://doi.org/10.1021/acs.jpcb.8b06493.

(18) Berlinger, S. A.; Dudenas, P. J.; Bird, A.; Chen, X.; Freychet, G.; McCloskey, B. D.; Kusoglu, A.; Weber, A. Z. Impact of Dispersion Solvent on Ionomer Thin Films and Membranes. *ACS Appl Polym Mater* **2020**, *2* (12), 5824–5834. https://doi.org/10.1021/acsapm.0c01076.

(19) Ngo, T. T.; Yu, T. L.; Lin, H. L. Influence of the Composition of Isopropyl Alcohol/Water Mixture Solvents in Catalyst Ink Solutions on Proton Exchange Membrane Fuel Cell Performance. *J Power Sources* **2013**, *225*, 293–303. https://doi.org/10.1016/j.jpowsour.2012.10.055.
(20) Mabuchi, T.; Huang, S. F.; Tokumasu, T. Nafion Ionomer Dispersion in Mixtures of 1-Propanol and Water Based on the Martini Coarse-Grained Model. *Journal of Polymer Science* **2020**, *58* (3), 487–499. https://doi.org/10.1002/pol.20190101.
(21) Mabuchi, T.; Huang, S. F.; Tokumasu, T. Dispersion of Nafion Ionomer Aggregates in 1-Propanol/Water Solutions: Effects of Ionomer Concentration, Alcohol Content, and Salt Addition. *Macromolecules* **2020**, *53* (9), 3273–3283. https://doi.org/10.1021/acs.macromol.9b02725.
(22) Gao, X.; Yamamoto, K.; Hirai, T.; Ohta, N.; Uchiyama, T.; Watanabe, T.; Imai, H.; Sugawara, S.; Shinohara, K.; Uchimoto, Y. Impact of the Composition of Alcohol/Water Dispersion on the Proton Transport and Morphology of Cast Perfluorinated Sulfonic Acid Ionomer Thin Films. *ACS Omega* **2021**, *6* (22), 14130–14137. https://doi.org/10.1021/acsomega.1c00607.
(23) Banerjee, S.; Curtin, D. E. Nafion® Perfluorinated Membranes in Fuel Cells. *J Fluor Chem* **2004**, *125* (8), 1211–1216. https://doi.org/10.1016/j.jfluchem.2004.05.018.
(24) Lin, H. L.; Yu, T. L.; Huang, C. H.; Lin, T. L. Morphology Study of Nafion Membranes Prepared by Solutions Casting. *J Polym Sci B Polym Phys* **2005**, *43* (21), 3044–3057. https://doi.org/10.1002/polb.20599.
(25) Su, G. M.; Cordova, I. A.; Yandrasits, M. A.; Lindell, M.; Feng, J.; Wang, C.; Kusoglu, A. Chemical and Morphological Origins of Improved Ion Conductivity in Perfluoro Ionene Chain Extended Ionomers. *J Am Chem Soc* **2019**, *141* (34), 13547–13561. https://doi.org/10.1021/jacs.9b05322.
(26) Gebel, G.; Diat, O. Neutron and X-Ray Scattering: Suitable Tools for Studying Lonomer Membranes. *Fuel Cells* **2005**, *5* (2), 261–276. https://doi.org/10.1002/fuce.200400080.
(27) Rubata, L.; Diat, O. Stretching Effect on Nafion Fibrillar Nanostructure. *Macromolecules* **2007**, *40* (26), 9455–9462. https://doi.org/10.1021/ma070362s.
(28) Eastman, S. A.; Kim, S.; Page, K. A.; Rowe, B. W.; Kang, S.; Soles, C. L.; Yager, K. G. Effect of Confinement on Structure, Water Solubility, and Water Transport in Nafion Thin Films. *Macromolecules* **2012**, *45* (19), 7920–7930. https://doi.org/10.1021/ma301289v.
(29) Rubatat, L.; Rollet, A. L.; Gebel, G.; Diat, O. Evidence of Elongated Polymeric Aggregates in Nafion. *Macromolecules* **2002**, *35* (10), 4050–4055. https://doi.org/10.1021/ma011578b.
(30) Kim, Y. S.; Welch, C. F.; Hjelm, R. P.; Mack, N. H.; Labouriau, A.; Orler, E. B. Origin of Toughness in Dispersion-Cast Nafion Membranes. *Macromolecules* **2015**, *48* (7), 2161–2172. https://doi.org/10.1021/ma502538k.
(31) Crothers, A. R.; Kusoglu, A.; Radke, C. J.; Weber, A. Z. Influence of Mesoscale Interactions on Proton, Water, and Electrokinetic Transport in Solvent-Filled Membranes: Theory and Simulation. *Langmuir* **2022**. https://doi.org/10.1021/acs.langmuir.2c00706.
(32) Collins, B. A.; Gann, E. Resonant Soft X-Ray Scattering in Polymer Science. *Journal of Polymer Science* **2022**, *60* (7), 1199–1243. https://doi.org/10.1002/pol.20210414.
(33) Liu, F.; Brady, M. A.; Wang, C. Resonant Soft X-Ray Scattering for Polymer Materials. *European Polymer Journal*. Elsevier Ltd August 1, 2016, pp 555–568. https://doi.org/10.1016/j.eurpolymj.2016.04.014.
(34) Su, G. M.; White, W.; Renna, L. A.; Feng, J.; Ardo, S.; Wang, C. Photoacid-Modified Nafion Membrane Morphology Determined by Resonant X-Ray Scattering and Spectroscopy. *ACS Macro Lett* **2019**, *8* (10), 1353–1359. https://doi.org/10.1021/acsmacrolett.9b00622.
(35) Luo, X.; Lau, G.; Tesfaye, M.; Arthurs, C. R.; Cordova, I.; Wang, C.; Yandrasits, M.; Kusoglu, A. Thickness Dependence of Proton-Exchange-Membrane Properties. *J Electrochem Soc* **2021**, *168* (10), 104517. https://doi.org/10.1149/1945-7111/ac2973.
(36) Shi, S.; Weber, A. Z.; Kusoglu, A. STRUCTURE-TRANSPORT RELATIONSHIP OF PERFLUOROSULFONIC-ACID MEMBRANES IN DIFFERENT CATIONIC FORMS. *Electrochim Acta* **2016**, *220*, 517–528. https://doi.org/10.1016/j.electacta.2016.10.096.

(37) Pandolfi, R. J.; Allan, D. B.; Arenholz, E.; Barroso-Luque, L.; Campbell, S. I.; Caswell, T. A.; Blair, A.; De Carlo, F.; Fackler, S.; Fournier, A. P.; Freychet, G.; Fukuto, M.; Gürsoy, D.; Jiang, Z.; Krishnan, H.; Kumar, D.; Kline, R. J.; Li, R.; Liman, C.; Marchesini, S.; Mehta, A.; N'Diaye, A. T.; Parkinson, D. Y.; Parks, H.; Pellouchoud, L. A.; Perciano, T.; Ren, F.; Sahoo, S.; Strzalka, J.; Sunday, D.; Tassone, C. J.; Ushizima, D.; Venkatakrishnan, S.; Yager, K. G.; Zwart, P.; Sethian, J. A.; Hexemer, A. Xi-Cam: A Versatile Interface for Data Visualization and Analysis. *J Synchrotron Radiat* **2018**, *25* (4), 1261–1270. https://doi.org/10.1107/S1600577518005787.

(38) Ye, X.; Zhu, C.; Ercius, P.; Raja, S. N.; He, B.; Jones, M. R.; Hauwiller, M. R.; Liu, Y.; Xu, T.; Alivisatos, A. P. Structural Diversity in Binary Superlattices Self-Assembled from Polymer-Grafted Nanocrystals. *Nat Commun* **2015**, *6*, 1–10. https://doi.org/10.1038/ncomms10052.

(39) Vijayakumar, M.; Govind, N.; Li, B.; Wei, X.; Nie, Z.; Thevuthasan, S.; Sprenkle, V.; Wang, W. Aqua-Vanadyl Ion Interaction with Nafion® Membranes. *Front Energy Res* **2015**, *3* (MAR), 1–5. https://doi.org/10.3389/fenrg.2015.00010.

(40) Risberg, E. D.; Eriksson, L.; Mink, J.; Pettersson, L. G. M.; Skripkin, M. Y.; Sandström, M. Sulfur X-Ray Absorption and Vibrational Spectroscopic Study of Sulfur Dioxide, Sulfite, and Sulfonate Solutions and of the Substituted Sulfonate Ions X3CSO3- (X = H, Cl, F). *Inorg Chem* **2007**, *46* (20), 8332–8348. https://doi.org/10.1021/ic062440i.

(41) Isegawa, K.; Nagami, T.; Jomori, S.; Yoshida, M.; Kondoh, H. In Situ S-K XANES Study of Polymer Electrolyte Fuel Cells: Changes in the Chemical States of Sulfonic Groups Depending on Humidity. *Physical Chemistry Chemical Physics* **2016**, *18* (36), 25183–25190. https://doi.org/10.1039/c6cp04052g.

(42) Rubatat, L.; Gebel, G.; Diat, O. Fibrillar Structure of Nafion: Matching Fourier and Real Space Studies of Corresponding Films and Solutions. *Macromolecules* **2004**, *37* (20), 7772–7783. https://doi.org/10.1021/ma049683j.

(43) Li, Y.; Peiffer, D. G.; Chu, B. Long-Range Inhomogeneities in Sulfonated Polystyrene Ionomers. *Macromolecules* **1993**, *26* (15), 4006–4012. https://doi.org/10.1021/ma00067a042.

(44) Gebel, G.; Moore, R. B. Small-Angle Scattering Study of Short Pendant Chain Perfuorosulfonated Lonomer Membranes. *Macromolecules* **2000**, *33* (13), 4850–4855. https://doi.org/10.1021/ma9912709.

(45) Liu, Y.; Horan, J. L.; Schlichting, G. J.; Caire, B. R.; Liberatore, M. W.; Hamrock, S. J.; Haugen, G. M.; Yandrasits, M. A.; Seifert, S.; Herring, A. M. A Small-Angle X-Ray Scattering Study of the Development of Morphology in Films Formed from the 3M Perfluorinated Sulfonic Acid Ionomer. *Macromolecules* **2012**, *45* (18), 7495–7503. https://doi.org/10.1021/ma300926e.

(46) Eikerling, M.; Kornyshev, A. A.; Spohr, E. Proton-Conducting Polymer Electrolyte Membranes: Water and Structure in Charge. In *Fuel Cells I*; Scherer, G. G., Ed.; Springer Berlin Heidelberg: Berlin, Heidelberg, 2008; pp 15–54. https://doi.org/10.1007/12_2008_132.

(47) Freychet, G.; Gann, E.; Thomsen, L.; Jiao, X.; McNeill, C. R. Resonant Tender X-Ray Diffraction for Disclosing the Molecular Packing of Paracrystalline Conjugated Polymer Films. *J Am Chem Soc* **2021**, *143* (3), 1409–1415. https://doi.org/10.1021/jacs.0c10721.

(48) Araki, T.; Ade, H.; Stubbs, J. M.; Sundberg, D. C.; Mitchell, G. E.; Kortright, J. B.; Kilcoyne, A. L. D. Resonant Soft X-Ray Scattering from Structured Polymer Nanoparticles. *Appl Phys Lett* **2006**, *89* (12). https://doi.org/10.1063/1.2356306.

(49) Crothers, A. R.; Kusoglu, A.; Radke, C. J.; Weber, A. Z. Influence of Mesoscale Interactions on Proton, Water, and Electrokinetic Transport in Solvent-Filled Membranes: Theory and Simulation. *Langmuir* **2022**. https://doi.org/10.1021/acs.langmuir.2c00706.

(50) Baker, A. M.; Crothers, A. R.; Chintam, K.; Luo, X.; Weber, A. Z.; Borup, R. L.; Kusoglu, A. Morphology and Transport of Multivalent Cation-Exchanged Ionomer Membranes Using Perfluorosulfonic Acid-Cez+as a Model System. *ACS Appl Polym Mater* **2020**, *2* (8), 3642–3656. https://doi.org/10.1021/acsapm.0c00633.

(51) Kusoglu, A.; Vezzù, K.; Hegde, G. A.; Nawn, G.; Motz, A. R.; Sarode, H. N.; Haugen, G. M.; Yang, Y.; Seifert, S.; Yandrasits, M. A.; Hamrock, S.; Maupin, C. M.; Weber, A. Z.; Di Noto, V.;

Herring, A. M. Transport and Morphology of a Proton Exchange Membrane Based on a Doubly Functionalized Perfluorosulfonic Imide Side Chain Perflourinated Polymer. *Chemistry of Materials* **2020**, *32* (1), 38–59. https://doi.org/10.1021/acs.chemmater.8b05012.

(52) Bird, A.; Lindell, M.; Kushner, D. I.; Haug, A.; Yandrasits, M.; Kusoglu, A. Modulating Perfluorinated Ionomer Functionality via Sidechain Chemistry. *Adv Funct Mater* **2024**. https://doi.org/10.1002/adfm.202311073.

(53) Luo, X.; Kushner, D. I.; Kusoglu, A. Anion Exchange Membranes: The Effect of Reinforcement in Water and Electrolyte. *J Memb Sci* **2023**, *685*. https://doi.org/10.1016/j.memsci.2023.121945.

(54) Tesfaye, M.; Kushner, D. I.; Kusoglu, A. Interplay between Swelling Kinetics and Nanostructure in Perfluorosulfonic Acid Thin-Films: Role of Hygrothermal Aging. *ACS Appl Polym Mater* **2019**, *1* (4), 631–635. https://doi.org/10.1021/acsapm.9b00005.

(55) Jung, J.; Lim, K. H.; Maurya, S.; Manriquez, L. D.; Atanasov, V.; Ahn, C. H.; Hwang, S. S.; Lee, A. S.; Kim, Y. S. Dispersing Agents Impact Performance of Protonated Phosphonic Acid High-Temperature Polymer Electrolyte Membrane Fuel Cells. *ACS Energy Lett* **2022**, 1642–1647. https://doi.org/10.1021/acsenergylett.2c00359.

(56) Münchinger, A.; Kreuer, K. D. Selective Ion Transport through Hydrated Cation and Anion Exchange Membranes I. The Effect of Specific Interactions. *J Memb Sci* **2019**, *592*. https://doi.org/10.1016/j.memsci.2019.117372.

(57) Wu, D.; Paddison, S. J.; Elliott, J. A.; Hamrock, S. J. Mesoscale Modeling of Hydrated Morphologies of 3m Perfluorosulfonic Acid-Based Fuel Cell Electrolytes. *Langmuir* **2010**, *26* (17), 14308–14315. https://doi.org/10.1021/la102358y.

(58) Wu, D.; Paddison, S. J.; Elliott, J. A. Effect of Molecular Weight on Hydrated Morphologies of the Short-Side-Chain Perfluorosulfonic Acid Membrane. *Macromolecules* **2009**, *42* (9), 3358–3367. https://doi.org/10.1021/ma900016w.